This article was downloaded by:
On: *25 January 2011*
Access details: *Access Details: Free Access*
Publisher *Taylor & Francis*
Informa Ltd Registered in England and Wales Registered Number: 1072954 Registered office: Mortimer House, 37-41 Mortimer Street, London W1T 3JH, UK

Liquid Crystals
Publication details, including instructions for authors and subscription information:
http://www.informaworld.com/smpp/title~content=t713926090

Liquid crystal phase diagram of the Gay-Berne fluid by density functional theory

Valeriy V. Ginzburg; Matthew A. Glaser; Noel A. Clark

Online publication date: 06 August 2010

To cite this Article Ginzburg, Valeriy V. , Glaser, Matthew A. and Clark, Noel A.(1997) 'Liquid crystal phase diagram of the Gay-Berne fluid by density functional theory', Liquid Crystals, 23: 2, 227 — 234
To link to this Article: DOI: 10.1080/026782997208488
URL: http://dx.doi.org/10.1080/026782997208488

PLEASE SCROLL DOWN FOR ARTICLE

Full terms and conditions of use: http://www.informaworld.com/terms-and-conditions-of-access.pdf

This article may be used for research, teaching and private study purposes. Any substantial or systematic reproduction, re-distribution, re-selling, loan or sub-licensing, systematic supply or distribution in any form to anyone is expressly forbidden.

The publisher does not give any warranty express or implied or make any representation that the contents will be complete or accurate or up to date. The accuracy of any instructions, formulae and drug doses should be independently verified with primary sources. The publisher shall not be liable for any loss, actions, claims, proceedings, demand or costs or damages whatsoever or howsoever caused arising directly or indirectly in connection with or arising out of the use of this material.

LIQUID CRYSTALS, 1997, VOL. 23, NO. 2, 227–234

Liquid crystal phase diagram of the Gay–Berne fluid by density functional theory

by VALERIY V. GINZBURG,* MATTHEW A. GLASER
and NOEL A. CLARK
Department of Physics, University of Colorado, Boulder CO 80309-0390, U.S.A.

(*Received 12 February 1997; accepted 12 March 1997*)

We calculate the liquid crystal phase diagram for a model fluid with Gay–Berne interparticle potential using the Tarazona smoothed-density approximation of density functional theory. Vapour, liquid, nematic and smectic A phases are considered. For length to breadth ratio $\kappa = 3$ and energy anisotropy $\kappa' = 5$, comparison with the simulation data of de Miguel *et al.* shows reasonable agreement.

Downloaded At: 20:29 25 January 2011

1. Introduction

The problem of prediction of phase behaviour of liquid crystals based on information about molecular shape and intermolecular interactions remains one of the most fundamental in liquid crystal physics. Traditional Onsager [1] and Maier–Saupe [2] theories described the nematic–isotropic transition qualitatively; de Gennes [3] and McMillan [4] proposed phenomenological theories for the nematic–smectic A transition as well. Although correctly describing the physics of both transitions, these theories do not rely specifically on information about intermolecular interactions and thus require additional assumptions and parameters to describe real materials (in de Gennes–McMillan theory, for example, smectic period must be introduced by hand rather than following from molecular information). Thus, for practical purposes, there exists a need for a universal molecular theory that can predict a phase diagram for a given material. The density functional theory (DFT) approach has so far been the most successful in this direction.

Application of DFT to liquid crystals has been mainly concentrated on lyotropic or hard-particle fluids [5]. It was based upon the quasi-exact knowledge of the equation of state for a hard-sphere fluid (Carnahan–Starling equation) [6], and the correspondence between the system of parallel hard ellipsoids and that of hard spheres (one can be converted into the other by an affine transformation—an observation made by Frenkel [7]). Any liquid crystalline fluid is considered to be 'close' to an equivalent system of hard ellipsoids, and its free energy functional is derived from that of hard spheres. Combined with the weighted-density approximation (which suggests that in a non-uniform phase like a smectic or a crystal, local steric energy depends not on the local mass density, but on a density averaged over some region according to some specific rules—for more details see Tarazona [8]), this approach resulted in qualitatively (and, in some cases, quantitatively) correct phase diagrams for hard ellipsoids [9], hard spherocylinders [10–12] and oblique hard spherocylinders [11].

To study phase diagrams for thermotropic liquid crystals, it was necessary to select a reasonable interparticle potential, i.e. one having appropriate symmetry which is, at the same time, computationally inexpensive. Mederos and Sullivan [13] considered a general potential consisting of isotropic, dipolar and quadrupolar parts, and calculated its phase diagram using DFT. However, lack of computational data on the Mederos–Sullivan potential makes it difficult to compare this result with either experimental or computational data. Moreover, the structure of their potential and density functional seems to be applicable only for rather small elongations, and it is unclear whether this approach can be extended to longer particles.

In recent years, the most studied potential describing interactions between anisotropic particles has been the Gay–Berne (GB) potential [14]. Gay and Berne proposed a function that described a van der Waals interaction energy between prolate or oblate uniaxial ellipsoids of revolution. Both shape and energy anisotropy appear in the potential in a rather natural way, thus allowing them to be varied at ease. Moreover, using the Weeks, Chandler and Andersen (WCA) prescription [15], one can easily separate the GB potential into a

*Author for correspondence.

0267–8292/97 $12·00 © 1997 Taylor & Francis Ltd.

repulsive (steric) part and an attractive part and study the relative role of both parts in phase formation.

The thermodynamics of Gay–Berne fluids has been investigated thoroughly through a number of computer simulation studies (both Monte Carlo and molecular dynamics). De Miguel *et al.* [16–18] calculated a phase diagram for specific values of shape and energy anisotropy to find such phases as isotropic vapour, isotropic liquid, nematic, smectic B and crystal. In another simulation for a slightly different parametrization of the potential, Luckhurst *et al.* [19, 20] also found a smectic A phase. In addition, a simulation of a repulsive (WCA) system of Gay–Berne ellipsoids was performed to show only isotropic and nematic phases (a crystal phase must exist at higher packing fractions, but the simulation was not extended to this region), in agreement with Frenkel's argument that hard ellipsoids do not form smectic phases. These data provide an excellent source of information for any thermodynamic theory and make the GB fluid an important test for molecular theories of liquid crystals. To date, several attempts have been made to describe the GB phase behaviour theoretically. Ginzburg *et al.* [21] analysed the behaviour of the nematic–isotropic transition in a GB system using the second virial approximation. Velasco *et al.* [22] applied the density functional formalism to achieve a quantitative agreement with simulation data for a nematic–isotropic transition.

In this article, we describe the application of a DFT method, similar to that of Velasco *et al.* [22], to the isotropic–nematic–smectic phase diagram of GB fluids. We analyse the role of attractive interactions in the formation of a smectic phase and compare the results with computer simulation data. We also calculate, for the first time, a temperature–pressure phase diagram.

Downloaded At: 20:29 25 January 2011

2. Free energy density functional

In this section, we briefly review density functional theory and its application to liquid crystals. The only complication that arises for liquid crystals compared with atomic fluids is that they may have both orientational and positional ordering. Thus, a particle is characterized not only by the position of its centre of mass $\mathbf{r}$, but also by a three-dimensional vector $\mathbf{n}$ describing its orientation. The single-particle distribution function (SDF) must be a function of both $\mathbf{r}$ and $\mathbf{n}$.

Within the DFT framework, the free energy is written as a functional depending on the SDF. It consists of the 'ideal gas' contribution and the 'interaction' contribution:

$$\beta F = \beta F_{\mathrm{id}} + \beta F_{\mathrm{int}}, \tag{1}$$

where

$$\beta F_{\mathrm{id}} = \int \mathrm{d}(1)\gamma(1)\ln\gamma(1), \tag{2}$$

$$\beta F_{\mathrm{int}} = \int \mathrm{d}(1)\gamma(1)\Psi_{\mathrm{hs}}(\bar{\rho}(\mathbf{r}_1))\frac{\int \mathrm{d}(2)\gamma(2)M(1,2)}{\int \mathrm{d}(\mathbf{r}_2)\rho(\mathbf{r}_2)M_{\mathrm{phe}}(\mathbf{r}_1-\mathbf{r}_2)} + \frac{1}{2}\int \mathrm{d}(1)\mathrm{d}(2)\gamma(1)\gamma(2)\Delta W_{\mathrm{att}}(1,2)g_{\mathrm{eff}}(1,2), \tag{3}$$

where the single particle distribution function $\gamma(1)$ depends on both orientational and translational degrees of freedom, and, in the arbitrary case of a system with a low symmetry

$$\gamma(1) = \rho(\mathbf{r}_1)f(\mathbf{r}_1, \mathbf{n}_1). \tag{4}$$

The first term of equation (3) describes repulsive hard-core steric interactions. This form of the steric energy was first proposed by Somoza and Tarazona [11] and is based on the hard-sphere equation of state (incorporated via the function Ψ_{hs}), the similarity between the hard-sphere system and the system of parallel hard ellipsoids, and the weighted density approximation (introduced via the smoothed density profile $\bar{\rho}(\mathbf{r})$). The definitions of functions Ψ_{hs}, $\bar{\rho}$, $M(1,2)$, and $M_{\mathrm{phe}}(\mathbf{r}_1-\mathbf{r}_2)$ are as follows:

$$\Psi_{\mathrm{hs}}(\bar{\rho}) = \frac{\eta(4-3\eta)}{(1-\eta)^2},\ \eta = \frac{\pi\bar{\rho}\sigma_0^2\sigma_z}{6}, \tag{5}$$

$$\bar{\rho}(\mathbf{r}) = \int \mathrm{d}\mathbf{s}\, w(|\mathbf{s}|;\bar{\rho}(\mathbf{r}))\rho(\mathbf{r}+\Sigma\mathbf{s}), \tag{6}$$

where σ_0 is the breadth of the particle, σ_z is its length, Σ is a diagonal matrix with elements $\sigma_0, \sigma_0, \sigma_z$ (in the coordinate system in which x, y, z coincide with the principal axes of the particle's inertia tensor); the Mayer function $M(1,2)$ is a step function and is equal to -1 if the two particles overlap and 0 if they do not overlap; $M_{\mathrm{phe}}(\mathbf{r}_1-\mathbf{r}_2)$ is a Mayer function for parallel hard ellipsoids, which, obviously, depends only on the relative positions of their centres of mass.

Equation (5) is a semi-empirical Carnahan–Starling equation of state for hard spheres (HS) [23]. Equation (6) is an integral equation for a smoothed density, with $w(|\mathbf{s}|;\bar{\rho}(\mathbf{r}))$ being a second-degree polynominal in $\bar{\rho}(\mathbf{r})$. The detailed description of function w and the ways to solve the integral equation (6) can be found in ref. [8]; for a brief summary, see Appendix A.

The second term of equation (3) describes the attractive intermolecular interactions, which, except for very low

temperatures and/or very high densities, are considered to be perturbations in the sense that, to the zeroth order approximation, they do not modify the pair correlation function. Thus, in equation (3), $g_{\text{eff}}(1,2)$ is calculated using the Parsons approximation [24] for hard particles:

$$g_{\text{eff}}(1,2) = g_{\text{hs}}(|\mathbf{r}_1 - \mathbf{r}_2|/\sigma(\mathbf{n1}, \mathbf{n2}, \hat{\mathbf{r}}_1 - \hat{\mathbf{r}}_2);\ \eta), \quad (7)$$

where g_{hs} is a HS PCF (see, e.g. [25]) described in detail in Appendix B, and packing fraction η is given by equation (5). The form of the attractive potential $\Delta W(1,2)$ will be described in detail in the next section.

We assume further that the orientational distribution function depends only upon $\mathbf{n}$, but not $\mathbf{r}$, i.e. orientational and translational degrees of freedom are separated (decoupling approximation). Although this approximation is not accurate in describing interlayer ordering in smectics (one can argue that between layers orientational ordering must be much weaker than within layers; see, for example, ref. [26]), the error in the free energy and other thermodynamic properties due to this inaccuracy should be insignificant, since most molecules are within layers. For positionally disordered phases, such as nematic and isotropic, of course, only orientational degrees of freedom remain.

Equations (2) to (7) constitute a complete definition of the free energy functional for all ordered and disordered phases. In order to analyse the phase behaviour of the system, one can use a variational approach and select specific trial functions for the single-particle density. For each phase (isotropic, nematic and smectic) it is possible to minimize the free energy with respect to the corresponding order parameters (if any), and then compare the free energies of all three phases to find the one that is thermodynamically stable. Further, one can calculate the pressure and chemical potential of each phase at a given density and temperature, and determine the coexistence regions between phases wherever necessary.

We parametrized the single particle density as follows:

$$f(\mathbf{n}) = \frac{\exp(\Lambda P_2(\mathbf{n}\hat{\mathbf{z}}))}{\int \mathrm{d}\mathbf{n} \exp(\Lambda P_2(\mathbf{n}\hat{\mathbf{z}}))}, \quad (8)$$

$$\rho(\mathbf{r}) = \frac{\exp(M \cos(2\pi z/D))}{\int \mathrm{d}z \exp(M \cos(2\pi z/D))}, \quad (9)$$

where Λ (orientational ordering strength), M (translational ordering strength), and D (smectic period) are parameters characterizing ordering. For the smectic phase, all three parameters are non-zero; for the nematic, Λ is positive and M is zero; for the isotropic phase, both Λ and M are zero.

3. Intermolecular potential

The Gay–Berne intermolecular potential is one of the most widely used in computer modelling of anisotropic liquids. It is parametrized as follows:

$$U_{\text{gb}}(1,2) = 4\varepsilon(1,2)\left\{\left[\frac{\sigma_0}{r_{12} + \sigma_0 - \sigma(1,2)}\right]^{12} - \left[\frac{\sigma_0}{r_{12} + \sigma_0 - \sigma(1,2)}\right]^{6}\right\}, \quad (10)$$

where $r_{12} = |\mathbf{r}_1 - \mathbf{r}_2|$, and configuration-dependent functions $\varepsilon(1,2)$ and $\sigma(1,2)$ are given by:

$$\sigma(1,2) = \sigma_0\left\{1 - \frac{\chi}{2}\left[\frac{(\hat{\mathbf{r}}_{12}\ \mathbf{n}_1 + \hat{\mathbf{r}}_{12}\ \mathbf{n}_2)^2}{1 + \chi \mathbf{n}_1\ \mathbf{n}_2} + \frac{(\hat{\mathbf{r}}_{12}\ \mathbf{n}_1 - \hat{\mathbf{r}}_{12}\ \mathbf{n}_2)^2}{1 - \chi \mathbf{n}_1\ \mathbf{n}_2}\right]\right\}, \quad (11)$$

$$\varepsilon(1,2) = \varepsilon_0 \varepsilon_1^{\nu}(\mathbf{n}_1, \mathbf{n}_2, \hat{\mathbf{r}}_{12}), \quad (12)$$

$$\varepsilon_1(\mathbf{n}_1, \mathbf{n}_2) = [1 - \chi^2(\mathbf{n}_1\ \mathbf{n}_2)^2]^{-1/2}, \quad (13)$$

$$\varepsilon_2(\mathbf{n}_1, \mathbf{n}_2, \hat{\mathbf{r}}_{12}) = \left\{1 - \frac{\chi'}{2}\left[\frac{(\hat{\mathbf{r}}_{12}\ \mathbf{n}_1 + \hat{\mathbf{r}}_{12}\ \mathbf{n}_2)^2}{1 + \chi' \mathbf{n}_1\ \mathbf{n}_2} + \frac{(\hat{\mathbf{r}}_{12}\ \mathbf{n}_1 - \hat{\mathbf{r}}_{12}\ \mathbf{n}_2)^2}{1 - \chi' \mathbf{n}_1\ \mathbf{n}_2}\right]\right\}. \quad (14)$$

Parameters χ and χ' are related to shape anisotropy κ (length to breadth ratio) and energy anisotropy κ' (side by side energy to end to end energy ratio) as:

$$\chi = \frac{\kappa^2 - 1}{\kappa^2 + 1}, \quad (15)$$

$$\chi' = \frac{\kappa'^{1/\mu} - 1}{\kappa'^{1/\mu} + 1}. \quad (16)$$

In the original paper by Gay and Berne [14], as well as in Monte Carlo simulations by de Miguel *et al.* [16–18], and in the first density functional theory of GB systems by Velasco *et al.* [22], the following set of parameters was used: $\kappa = 3$, $\kappa' = 5$, $\mu = 2$, $\nu = 1$. We will use the same values in our calculation of the phase diagram.

As proposed by Mo and Gubbins [27], one can split the van der Waals type potential into the reference repulsive part and perturbation attractive part. For the case of the GB potential, such an operation yields:

$$U_0(1,2) = \begin{cases} u_{\text{gb}}(1,2) + \varepsilon(1,2), & \text{if } r_{12} < r_{\text{m}}(\mathbf{n}_1, \mathbf{n}_2) \\ 0, & \text{if } r_{12} \geqslant r_{\text{m}}(\mathbf{n}_1, \mathbf{n}_2), \end{cases} \quad (17)$$

$$\Delta W_{\text{att}}(1,2) = \begin{cases} -\varepsilon(1,2), & \text{if } r_{12} < r_{\text{m}}(\mathbf{n}_1, \mathbf{n}_2) \\ u_{\text{gb}}(1,2), & \text{if } r_{12} \geqslant r_{\text{m}}(\mathbf{n}_1, \mathbf{n}_2), \end{cases} \quad (18)$$

Downloaded At: 20:29 25 January 2011

where $r_m(\mathbf{n}_1, \mathbf{n}_2) = (2^{1/6} - 1)\sigma_0 + \sigma(1, 2)$ is the orientational-dependent position of the minimum; the function $\Delta W_{att}(1, 2)$ is the one to be used in the free energy functional (3). Finally, the repulsive potential energy (17) is replaced by a hard Gaussian overlap (HGO) potential:

$$U_0(1, 2) = \infty, \quad \text{if } r_{12} < \sigma(1, 2)$$
$$0, \quad \text{if } r_{12} \geqslant \sigma(1, 2). \tag{19}$$

In the next section, we will present results of the phase diagram calculation and compare it with the simulation data.

4. Results and discussion

4.1. *Calculation details*

We calculated the free energy integral using a grid in a five-dimensional variable space with four meshpoints for azimuthal angle, 20 for polar angle, and 16 meshpoints for each spatial dimension (X, Y and Z). The simple trapezoidal rule was used for integration. The parameter space consisted of two order parameters: the nematic order parameter $S = \langle P_2(\cos(\theta)) \rangle$, and the smectic order parameter $\tau = \langle \cos(2\pi z/D) \rangle$, as well as the smectic period D itself. For prolate ellipsoids, $0 \leqslant S \leqslant 1$, and $0 \leqslant \tau \leqslant 1$ is always true with a correct selection of the reference frame. We used 12 equally spaced meshpoints in the interval [0, 1] for both order parameters, and evaluated free energies for these values of S and τ. Units of length and energy were selected so that $\varepsilon_0 = 1$, $\sigma_0 = 1$; thus the units of pressure and density are $\varepsilon_0 \sigma_0^{-3}$ and σ_0^{-3}, respectively. The smectic period D was assumed to be in the range [2·4 to 3·9] in reduced length units (compare with the particle length of 3·0), and at every point, minimization with respect to D was performed. To find the smectic state, the discrete analogue of the steepest descent method was used and the most ordered minimum was taken to represent the smectic state.

Calculations were performed on a Silicon Graphics Indigo 2 R4400 workstation. After the preparation of initial lookup tables for Mayer functions and potential energy, we performed repeated loops over temperature and density. At each temperature point, free energy minimization was performed for 80 densities in the range [0 to 0·4] in reduced density units. Coexistence densities and transition points were found using the Maxwell construction. The calculation was repeated for 30 temperatures in the range [0·3 to 1·2] in reduced energy units. Calculation of the whole phase diagram took approximately two hours of cpu time.

4.2. *Hard Gaussian overlap*

In order to test the algorithm, we started with the calculation of the athermal phase diagram for the HGO system (no attractive interactions). The HGO fluid is very close to a system of hard ellipsoids which, as is known, does not exhibit smectic phases. We expected, therefore, to find only isotropic and nematic phases up to rather high densities; had the smectic phase been found, it would suggest that either the free energy functional itself or the numerical algorithm was inaccurate. The results (together with Monte Carlo simulation data from ref. [17]) are shown in figure 1, giving pressure versus density and both nematic and smectic order parameters versus density. It is easy to see that the smectic order parameter is zero for all densities, so no smectic phase appears. The isotropic–nematic transition occurs at $\rho = 0{\cdot}325$, in very good agreement with the simulations.

4.3. *Gay–Berne phase diagram*

In figure 2, the phase diagram for a Gay–Berne fluid is shown; solid lines correspond to the DFT calculations, and squares correspond to the Monte Carlo results of de Miguel *et al.* [17]. It can be seen that the agreement overall is rather satisfactory, although some discrepancy exists in the location of the triple point I–V–S (isotropic liquid–vapour–smectic): in the DFT calculations, it appears to be at somewhat higher temperature and lower density than in Monte Carlo simulation. The agreement for another triple point, I–N–S (isotropic–nematic–smectic), is slightly better, because it is located at higher temperatures, where mean-field-type theories like DFT usually accumulate fewer errors.

It is important to point out the ambiguity about the smectic phase. According to de Miguel *et al.* [17], the smectic phase observed in a GB fluid is hexatic B, not smectic A. The difference between the two is that hexatic B has a long range bond orientational ordering in the layer plane, while smectic A does not. Within the framework of our DFT , we were unable to characterize this in-plane ordering, and thus may have introduced additional energy costs associated with this omission (which may explain why the DFT estimate for the I–V–S triple point temperature was too low).

In figure 3, we show the pressure–density isotherm for $T = 0{\cdot}65$ (DFT results compared with Monte Carlo data) and the nematic and smectic order parameters for the same temperature. It can be seen on both curves that at this temperature, there is one strongly first order isotropic–smectic transition with a broad coexistence region. This feature is typical of all points below I–N–S triple points where there is no stable nematic phase.

In figure 4, the pressure-density isotherm and order parameters are shown for $T = 0{\cdot}95$, above the I–N–S triple point. Now it can be seen that there are two transitions, a weak first order isotropic–nematic transition and a second-order nematic–smectic transition. Such a

Downloaded At: 20:29 25 January 2011

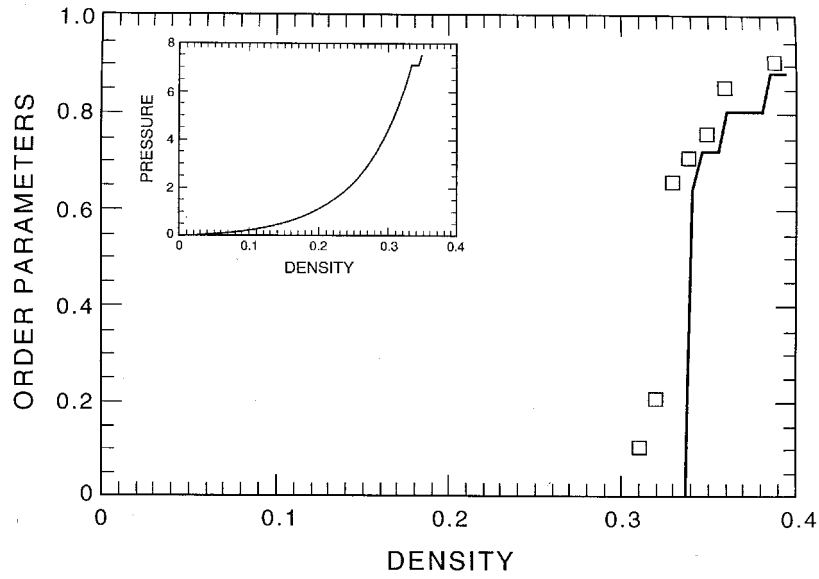

Figure 1. Density functional theory (solid curves) and Monte Carlo results from ref. [17] (squares) for the HGO system: nematic order parameter versus density. Inset: pressure versus density.

Downloaded At: 20:29 25 January 2011

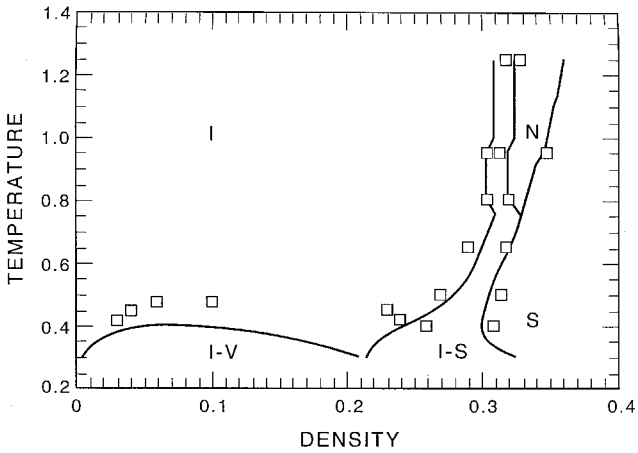

Figure 2. Temperature–density phase diagram of the Gay–Berne fluid with $\kappa = 3$, $\kappa' = 5$: density functional theory (solid lines) and Monte Carlo results (squares). Phases: I isotropic liquid. V vapour, N nematic, S smectic.

picture is clearly seen in the behaviour of the order parameters, where S jumps from 0 to 0·65 at $\rho = 0{\cdot}316$ and τ jumps only from 0 to 0·25 at $\rho = 0{\cdot}336$; it is also seen in the behaviour of the equation of state, where there is a slight discontinuity at the first transition, but only a small change in slope at the second.

Although one would expect that close to the triple point I–N–S, the nematic–smectic transition must be first order (this follows both from general thermodynamic principles and from de Gennes–McMillan theory [3,4] for this transition), we have not been able to observe this effect. This means that the coexistence region for the first-order nematic–smectic transition was always smaller than our density precision. In the future, it would be interesting to calculate the coefficients of the McMillan–de Gennes functional for this GB system and obtain an estimate for the size of the region where the transition is first order.

In figure 5, we show the pressure–temperature phase diagram. It has, as expected, a liquid–vapour line at small pressures that terminates at a critical point, and a smectic–isotropic line that branches into smectic–nematic and nematic–isotropic lines at higher pressures. Both of these lines continue indefinitely, since they separate phases of different symmetries.

5. Conclusions

We applied the density functional theory to describe the phase diagram of a Gay–Berne fluid (including the smectic A phase). The results obtained are in reasonable agreement with the results of Monte Carlo simulations. The most significant discrepancy (that in the temperature of the I–V–S triple point) can be explained by the possible difference between the hexatic B phase reported in Monte Carlo simulations and the smectic A phase assumed in the DFT calculation.

The speed and accuracy of the DFT method make it an important tool in the investigation of the thermodynamic properties of mesogenic materials. The reported results can be easily extended to the case of particles with arbitrary shape and energy anisotropies, and thus allow a simple and direct study of the dependence of the stability of both nematic and smectic phases upon these two parameters. It should also be possible in the future

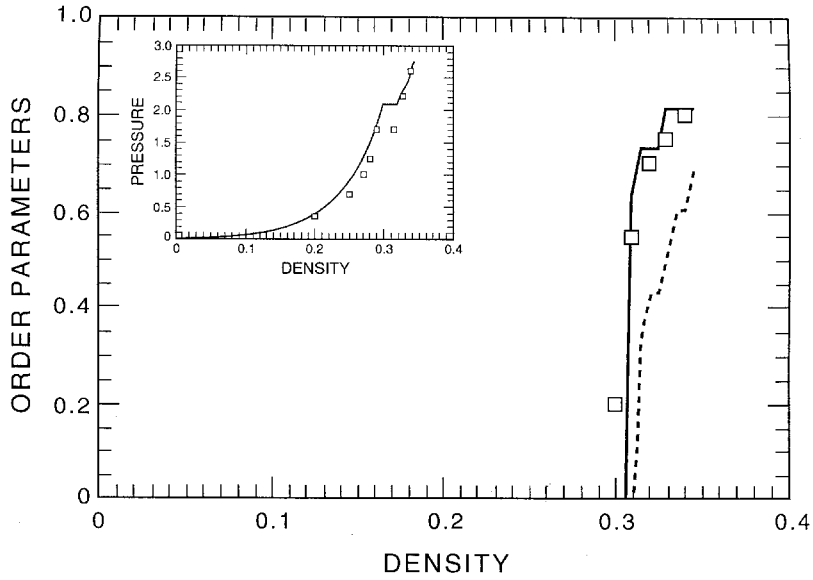

Figure 3. Pressure–density isotherm (inset) and order parameters (orientational—solid line, translational—dashed line) for $T = 0{\cdot}65$. Squares correspond to selected points from Monte Carlo simulations for pressure and nematic order parameter.

Downloaded At: 20:29 25 January 2011

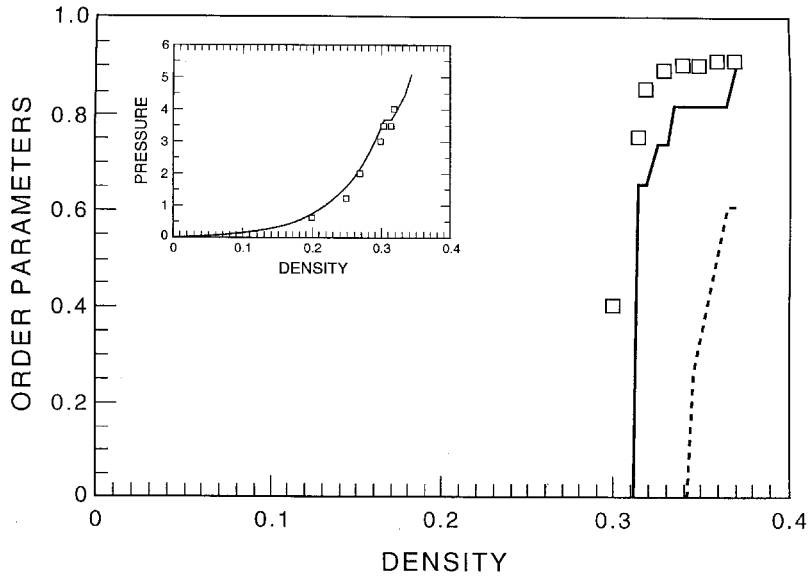

Figure 4. Same as figure 3, but for $T = 0{\cdot}95$.

to apply these results to predict phase behaviour of real anisotropic organic fluids, although the necessity to account for molecular flexibility will still be a very significant obstacle.

This work was sponsored by the NSF-MRG Grant DMR 92-02312.

Appendix A: Smoothed density function

The smoothed density function $\bar{\rho}(\mathbf{r})$ can be written as follows:

$$\bar{\rho} = \frac{2\bar{\rho}_0}{1 - \bar{\rho}_1 + \sqrt{[(1-\bar{\rho}_1)^2 - 4\bar{\rho}_0\bar{\rho}_2]^{1/2}}}, \tag{A1}$$

where the functions $\bar{\rho}_0$, $\bar{\rho}_1$, $\bar{\rho}_2$ are:

$$\bar{\rho}_0(\mathbf{r}) = \int \mathbf{ds}\, w_0(|\mathbf{s}|)\rho(\mathbf{r} + \Sigma\mathbf{s}); \tag{A2}$$

$$\bar{\rho}_1(\mathbf{r}) = \sigma_0^2\sigma_z \int \mathbf{ds}\, w_1(|\mathbf{s}|)\rho(\mathbf{r} + \Sigma\mathbf{s}); \tag{A3}$$

$$\bar{\rho}_2(\mathbf{r}) = (\sigma_0^2\sigma_z)^2 \int \mathbf{ds}\, w_2(|\mathbf{s}|)\rho(\mathbf{r} + \Sigma\mathbf{s}). \tag{A4}$$

The 'weight functions' w_0, w_1, w_2 are:

$$w_0(s) = \frac{3}{4\pi}\Theta(s), \tag{A5}$$

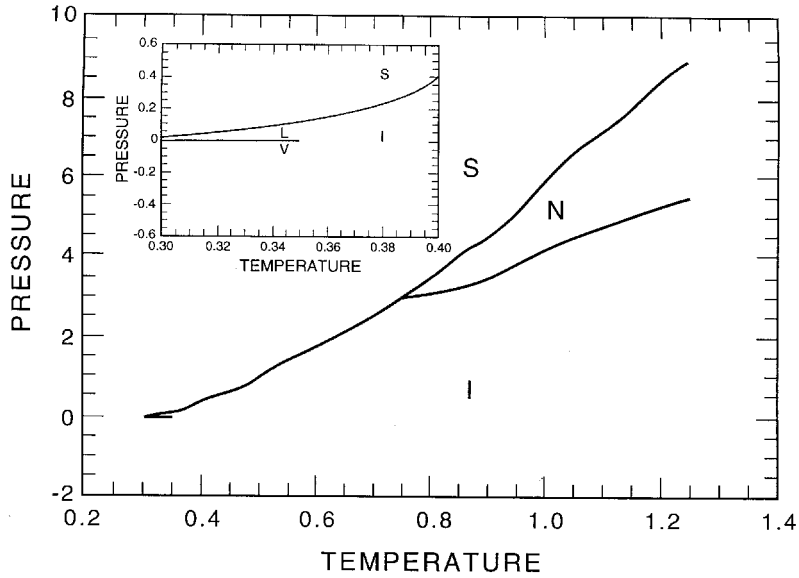

Figure 5. Temperature–pressure phase diagram of the Gay–Berne fluid. The inset shows an expanded view of the low-temperature region to demonstrate better the liquid–vapour coexistence. Phases: I isotropic (above critical temperature), L isotropic liquid, V isotropic vapour, N nematic, S smectic.

Downloaded At: 20:29 25 January 2011

$$w_2(s) = \frac{5}{4\pi}(6 - 12s + 5s^2)\Theta(s), \tag{A6}$$

$$w_1(s) = a_0 + a_1 s + a_2 s^2, \qquad \text{if } 0 < s \leqslant 1$$

$$c \exp[-\beta_1(s-1)\sin\alpha(s-1)] + \exp[-\beta_2(s-1)(b_0 + b_1 s + b_2 s^2 + b_3 s^3], \qquad \text{if } s > 1, \tag{A7}$$

with $\Theta(s) = 0$ if $s \leqslant 1$ and 1 if $s > 1$, and the coefficients in equation (A7) are: $a_0 = 0{\cdot}90724$, $a_1 = -1{\cdot}23717$, $a_2 = 0{\cdot}21616$, $c = 0{\cdot}10244$, $\beta_1 = 3{\cdot}5621$, $\beta_2 = 12{\cdot}0$, $\alpha = 4{\cdot}934$, $b_0 = 35{\cdot}124$, $b_1 = 98{\cdot}684$, $b_2 = 92{\cdot}693$, $b_3 = -29{\cdot}257$.

Appendix B: Pair correlation function

The pair correlation function $g_{hs}(x, \eta)$, where x is a dimensionless distance and η is a packing fraction, is given by the following Verlet fit, which rather closely approximates the solution of the Percus–Yevick equation:

$$g_{hs}(x, \eta) = [s_0 + s_1(x-1) + s_2(x-1)^2]/x^2, \tag{B1}$$

where

$$s_0 = \frac{1 - 0{\cdot}5\eta}{(1-\eta)^3}; \; s_1 = \frac{2 - 7{\cdot}5\eta + 0{\cdot}5\eta^2 - 5{\cdot}7865\eta^3 - 1{\cdot}51\eta^4}{(1-\eta)^4};$$

$$s_2 = \frac{2 - 20\eta + 30\eta^2 + 0{\cdot}17\eta^3 - 26{\cdot}796\eta^4 + 11{\cdot}2241\eta^5}{(1-\eta)^5}.$$

If $0 < x \leqslant 1$, then $g_{hs}(x, \eta) = 0$.

References

[1] Onsager, L., 1949, *Ann. N. Y. Acad. Sci.*, **51,** 62.
[2] Maier, W., and Saupe, A., 1958, *Z. Naturforsch.*, **A13,** 564; 1959, *ibid.*, **A14,** 882; 1960, *ibid.*, **A15,** 287.
[3] De Gennes, P. G., and Prost, J., 1993, *The Physics of Liquid Crystals*, 2nd Edn (Oxford: Clarendon Press), and references therein.
[4] McMillan, W. L., 1971, *Phys. Rev. A*, **4,** 1238.
[5] Vroege, G. J., and Lekkerkerker, H. N. W., 1992, *Rep. Prog. Phys.*, **55,** 1241.
[6] Hansen, J. P., and McDonald, I. R., 1986, *Theory of Simple Liquids* (London: Academic Press), and references therein.
[7] Frenkel, D., 1987, *Mol. Phys.*, **60,** 1, and references therein.
[8] Tarazona, P., 1985, *Phys. Rev. A*, **31,** 2673.
[9] Mulder, B., 1987, *Phys. Rev. A,* **35,** 3095.
[10] Poniewierski, A., and Holyst, R., 1988, *Phys. Rev. Lett.*, **61,** 2461.
[11] Somoza, A. M., and Tarazona, P., 1989, *J. chem. Phys.*, **91,** 517.
[12] Poniewierski, A., and Sluckin, T. J., 1991, *Mol. Phys.*, **73,** 199.
[13] Mederos, L., and Sullivan, D. E., 1989, *Phys. Rev. A*, **39,** 854.
[14] Gay, J. G., and Berne, B. J., 1981, *J. chem. Phys.*, **74,** 3316.
[15] Weeks, J. D., Chandler, D., and Andersen, H. C., 1971, *J. chem. Phys.*, **54,** 5237.
[16] De Miguel, E., Rull, L. F., Chalam, M. K., Gubbins, K. E., and van Swol, F., 1991, *Mol. Phys.*, **72,** 593.
[17] De Miguel, E., Rull, L. F., Chalam, M. K., and Gubbins, K. E., 1991, *Mol. Phys.*, **74,** 405.
[18] De Miguel, E., del Rio, E. M., Brown, J. T., and Allen, M. P., 1996, *J. chem. Phys.*, **105,** 4234.

[19] Hashim, R., Luckhurst, G. R., and Romano, S., 1995, *J. chem. Soc. Faraday Trans.*, **91,** 2141.
[20] Luckhurst, G. R., Stephens, R. A., and Phippen, R. W., 1990, *Liq. Cryst.*, **8,** 451.
[21] Ginzburg, V. V., Glaser, M. A., and Clark, N. A., 1996, *Liq. Cryst.*, **21,** 265.
[22] Velasco, E., Somoza, A. M., and Mederos, L., 1995, *J. chem. Phys.*, **102,** 8107.
[23] Carnahan, N. F., and Starling, K. E., 1969, *J. chem. Phys.*, **51,** 635.
[24] Parsons, J. D., 1979, *Phys. Rev. A*, **19,** 1225.
[25] Verlet, L., and Weis, J. J., 1972, *Mol. Phys.*, **24,** 1013.
[26] Van Roiji, R., Bolhuis, P., and Frenkel, D., 1995, *Phys. Rev. E*, **52,** R1277.
[27] Mo, K. C., and Gubbins, K. E., 1975, *J. chem. Phys.*, **63,** 1490.

Downloaded At: 20:29 25 January 2011